


## CASE REPORT

# Features of ophthalmic, magnetic resonance imaging, and histopathology of a feline case of idiopathic sclerosing orbital pseudotumor

Hao Lee<sup>1,2</sup> | Chih-Ching Wu<sup>2</sup> | Pei-Wen Liao<sup>2,3</sup> | Kunbee Michael Chang<sup>4</sup> |  
 Li-Ning Wei<sup>2,5</sup> | Yi-Ying Wu<sup>2,5</sup> | Man-Ha Chan<sup>1</sup> | Yi-Shan Chiang<sup>1</sup> |  
 Victor Fei Pang<sup>3</sup> | Chung-Tien Lin<sup>1,2</sup> 

<sup>1</sup>Institute of Veterinary Clinical Sciences, School of Veterinary Medicine, National Taiwan University, Taipei, Taiwan

<sup>2</sup>National Taiwan University Veterinary Hospital, Taipei, Taiwan

<sup>3</sup>Graduate Institute of Molecular and Comparative Pathobiology, School of Veterinary Medicine, National Taiwan University, Taipei, Taiwan

<sup>4</sup>Veterinary Eye Clinic, Alhambra, California, USA

<sup>5</sup>Vision Eyecare Center for Animals, Taipei, Taiwan

## Correspondence

Chung-Tien Lin, Institute of Veterinary Clinical Sciences, School of Veterinary Medicine, College of Bio-Resources and Agriculture, National Taiwan University No. 1, Section 4, Roosevelt Road, Taipei 106, Taiwan.  
 Email: [eyevet.lin@gmail.com](mailto:eyevet.lin@gmail.com)

Victor Fei Pang, Graduate Institute of Molecular and Comparative Pathobiology, School of Veterinary Medicine, College of Bio-Resources and Agriculture, National Taiwan University, Taipei, Taiwan.  
 Email: [pang@ntu.edu.tw](mailto:pang@ntu.edu.tw)

## Abstract

In the present report, we describe a case of sclerosing orbital pseudotumor in an 11-year-old castrated male American Shorthair cat. Ophthalmic exam showed lagophthalmos, retracted right upper eyelid, and resistant to retropulsion in his right eye. Under magnetic resonance imaging (MRI) scans, increased volume of the extraocular muscles (EOMs) of the right eye was prominent. Immunosuppressive dosage of prednisolone partially ameliorated the clinical signs, but some clinical signs were still gradually progressive or persistent. In the second MRI scan, decreased diameter of the thickened right extraocular muscles was found. After the third MRI scan, enucleation of the right eye was performed due to substantial adverse effects of systemic steroid therapy. Histopathological examination revealed no evidence of neoplastic transformation nor infection. Feline restrictive orbital myofibroblastic sarcoma (FROMS) was therefore excluded, suggesting unknown causes of extensive fibrotic changes in the right orbit of the affected cat.

## KEYWORDS

apparent diffusion coefficient (ADC) map, cat, diffusion-weighted imaging sequence, magnetic resonance imaging, MRI, orbital pseudotumor

## 1 | INTRODUCTION

Idiopathic sclerosing orbital inflammation (ISOI) is a progressive disease damaging the orbital structure by fibrotic tissue entrapment in human patients (Rootman et al., 1994). Pain, proptosis, eyelid swelling, and ptosis are common clinical signs in ISOI patients. Treatment out-

comes are often disappointing, and early and aggressive immunosuppressive therapy has been suggested (Rootman et al., 1994). Similar orbital manifestation of sclerosing disease was also reported in cats (Billson et al., 2006). A retrospective study by Billson et al. (2006) reviewed seven cases of feline idiopathic sclerosing orbital pseudotumor, including the clinical presentations, management, and pathologic

This is an open access article under the terms of the [Creative Commons Attribution-NonCommercial-NoDerivs](https://creativecommons.org/licenses/by-nc-nd/4.0/) License, which permits use and distribution in any medium, provided the original work is properly cited, the use is non-commercial and no modifications or adaptations are made.

© 2022 The Authors. *Veterinary Medicine and Science* published by John Wiley & Sons Ltd.



**FIGURE 1** Clinical signs of right upper eyelid retraction and progression of the right eye corneal granulation. (a) Photograph taken on the day of the first magnetic resonance imaging (MRI) scan. Obvious right upper eyelid retraction and mild lagophthalmos are seen in right eye. (b) Photograph taken on the day of the second MRI scan, approximately 1 month after the first MRI scan. Despite restarting immunosuppressive glucocorticoid therapy, the clinical signs progressed after initial improvement. (c) Photograph taken on the day of the third MRI scan, approximately 3 months after the first MRI scan. The right eye displays severe exposure keratopathy with extensive corneal granulation. The degree of the right eye lagophthalmos and upper eyelid retraction becomes worse in comparison with that of the second MRI scan

findings. The treatment responses were poor in all cases. All cats ultimately underwent enucleation surgery for symptom relief. And due to its progressive characteristic and unresponsiveness to therapy, most cats were euthanized (Billson et al., 2006). In the study of Bell et al. (2011), the term feline restrictive orbital myofibroblastic sarcoma was introduced to describe the aggressive nature and neoplastic course of the idiopathic sclerosing orbital disease in felines.

In this report, we present the clinical, magnetic resonance imaging (MRI), and histopathology features of a feline case with retracted right upper eyelid and reduced right eye retropulsion.

## 2 | CASE DESCRIPTION

### 2.1 | Clinical ophthalmic and MRI findings

An 11-year-old castrated male American Shorthair cat with retracted OD eyelids, OD corneal ulceration, and OD high intraocular pressure was referred to the ophthalmology clinic for ophthalmic evaluation.

The cat was obese (BCS 7/9, 5.98 kg) with normal spirit on physical examination. On ophthalmic examination, right eye lagophthalmos, obvious retracted right upper eyelid, and resistant to retropulsion were noted. Other abnormalities of the right eye included high intraocular pressure (HIOP, 31 mmHg), negative menace response, and corneal ulceration. The results of ophthalmic examination of the left eye were unremarkable. The values of blood examination were within normal limits. Drops of 0.3% Tobramycin eye drop (Tobrex, Alcon, U.S.A.) and 2% dorzolamide with 0.5% timolol eye drop (Cosopt, Laboratories Merck Sharp & Dohme-Chibret) were prescribed for the corneal ulceration and high intraocular pressure of the right eye. However, the clinical signs (Figure 1a) and HIOP (31–35 mmHg) were persistent and even worsened under eyedrops for the first 2 weeks of treatment.

The first MRI scan was performed (Figure 2). The sequences used for evaluation included T1-weighted (T1W), T2-weighted (T2W), T1-

weighted fat suppression (T1W FS), fluid-attenuated inversion recovery (FLAIR), spiral three-dimensional T1-weighted TFE (s3D T1W TFE), post contrast T1W, and post contrast s3D T1W TFE. In the scans, the most prominent finding was the increased volume of the extraocular muscles (EOMs) of the right eye, especially the medial and dorsal rectus muscles. In the slices that the diameter of the muscles can be clearly measured, the right medial rectus muscle was about 1.5 times larger than the left one. Through three-dimensional sequences, detailed evaluation of the lesion was made. The enlargement of the right EOMs was generally smooth and even from the origin to the insertion point. No focal mass lesion presented. Besides the EOMs, other structural abnormalities of the right eye including the protrusion of the bulbus oculi, decreased retrobulbar adipose tissue, increased size of anterior chamber and the thickness of sclera and cornea, which could be well appreciated in dorsal plane.

In a few areas within the EOMs, patchy hyperintensity in T1W images was noted. Markedly increased signal intensity of right extraocular muscles, sclera, and cornea of right eye in T2W, FLAIR, and fat stat sequences was noted. After intravenous gadolinium injection, those lesions were strongly contrast enhanced.

An oval cystic mass was found on the rostral-medial aspect of the right globe. It was composed of two parts. The lateral part was hyperintense in T2W images and the signal was voided in FLAIR sequence without contrast enhancement. The medial part was hyperintense in T1W, T2W, and fat stat images when it was compared to EOMs. Homogeneous enhancement was noted after contrast injection. Considering the aqueous secretion of the third eyelid gland in cats, the cystic mass was likely to be this structure, of which the outflow ducts were obstructed due to the periorbital soft tissue swelling. The orbit was intact, and no signs of bone lysis were found.

Right eye biopsy surgery was performed following an MRI scan under the same anaesthesia period. However, based on the MRI images, the affected tissue could not be approached easily without an enucleation surgery. Only the right bulbar conjunctiva near the retracted lateral canthus was incised for histopathological

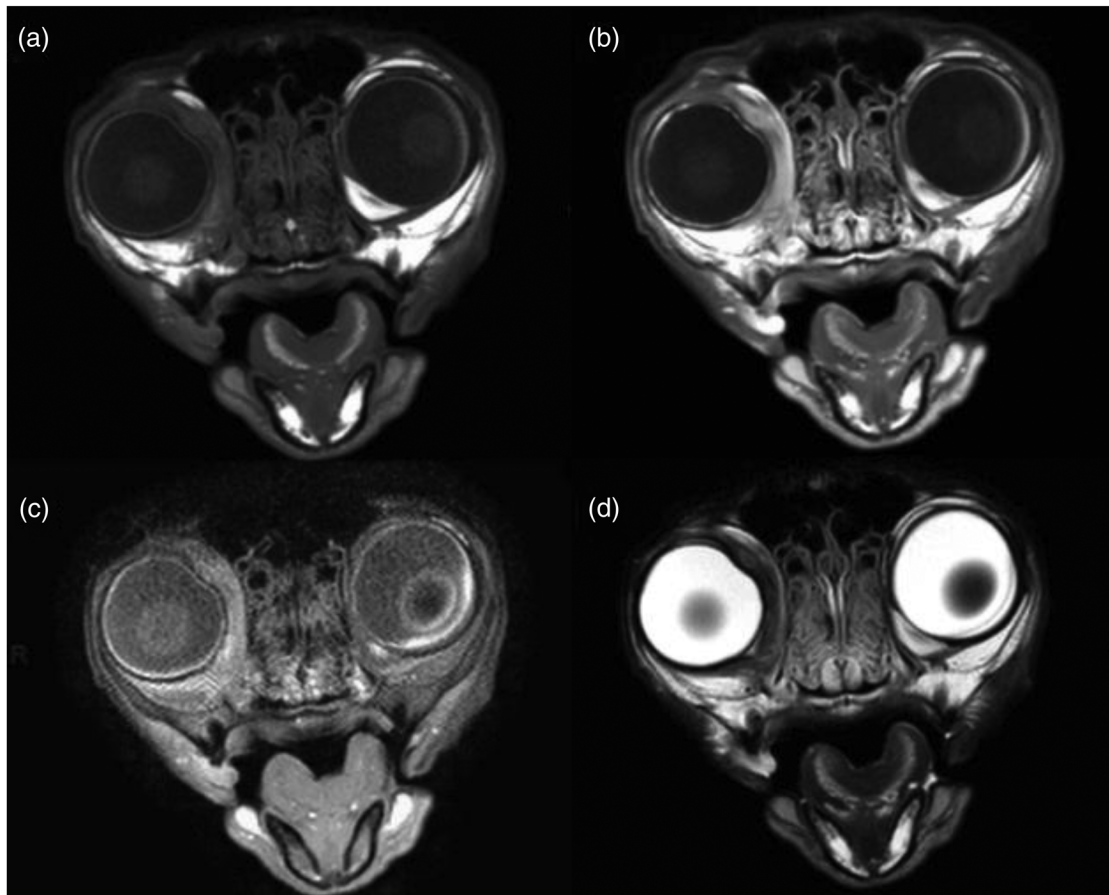


**FIGURE 2** The first magnetic resonance imaging (MRI) scan images. (a) T1-weighted sequence image. (b) T1-weighted contrast enhancement sequence image. (c) T1-weighted fat suppression sequence image. (d) T2-weighted sequence image. Increased signal intensity and thickness of the right eye periorbital tissue are seen under T1-weighted, T2-weighted, and T1-weighted fat suppression sequences. The affected soft tissues are most likely the right medial rectus muscle, dorsal oblique muscle, and ventral rectus muscle. The right eye periorbital tissue is strongly contrast-enhanced. The deformed right globe is likely caused by the pressure from the surrounding tissue

examination. The histopathological finding was conjunctivitis with prominent fibrosis and mild oedema.

According to the findings of the clinical presentation, ophthalmic examination, and the first MRI images, the differential diagnoses included idiopathic sclerosing orbital pseudotumor (ISOP), feline restrictive orbital myofibroblastic sarcoma (FROMS), and immune-mediated myositis. Prednisolone was prescribed after the first MRI examination. From the third week of the first presentation, an immunosuppressive dosage of steroid therapy at 2 mg/kg/day was given for 4 days, and the dosage was tapered to the anti-inflammatory dosage at 1 mg/kg/day for the following 4 days. After taking prednisolone for 1 week, the clinical signs of OD were improved, including returning to the reference range of OD intraocular pressure (17 mmHg), improved motility of eyelids and retropulsion of the globe, and more easily observed globe. The owner noticed reduced periorbital swelling and less deformed palpebral fissure when the cat was under the immunosuppressive dosage. However, the right upper eyelid retraction gradually worsened. Hence, the prednisolone was resumed to the immunosuppressive dose (2 mg/kg/day), and the dosage was adjusted based on the clinical signs and owner's observation weekly.

The second MRI scan was performed 1 month after the first MRI examination to determine the treatment response of steroid therapy when the cat had taken the immunosuppressive dosage of prednisolone at 2 mg/kg/day for 2 weeks. On the day of the second MRI scan, the clinical signs progressed after initial improvement (Figure 1b). When compared with the previous MRI images, the difference of signal intensity of bilateral EOMs in T2W images reduced, especially in segments closer to the muscle origins. Though the anatomic orientation of every slice was impossible to be the same between the first and second MRI scans, decreased diameter of the right extraocular muscles was found in most of the images in transverse and dorsal planes. The size of the enlarged right third eyelid gland reduced greatly (Figure 3), and the cystic mass found in the first MRI scan was not found in the second MRI scan.

After the second MRI examination, the prednisolone was readjusted to a higher immunosuppressive dosage at 4 mg/kg/day and tapered gradually from 4 mg/kg/day to 2 mg/kg/day over a course of 3 weeks.

While the clinical signs of the right eyelid retraction and lagophthalmos were stable under the higher immunosuppressive dosage of prednisolone, the OD keratitis and corneal granulation became more

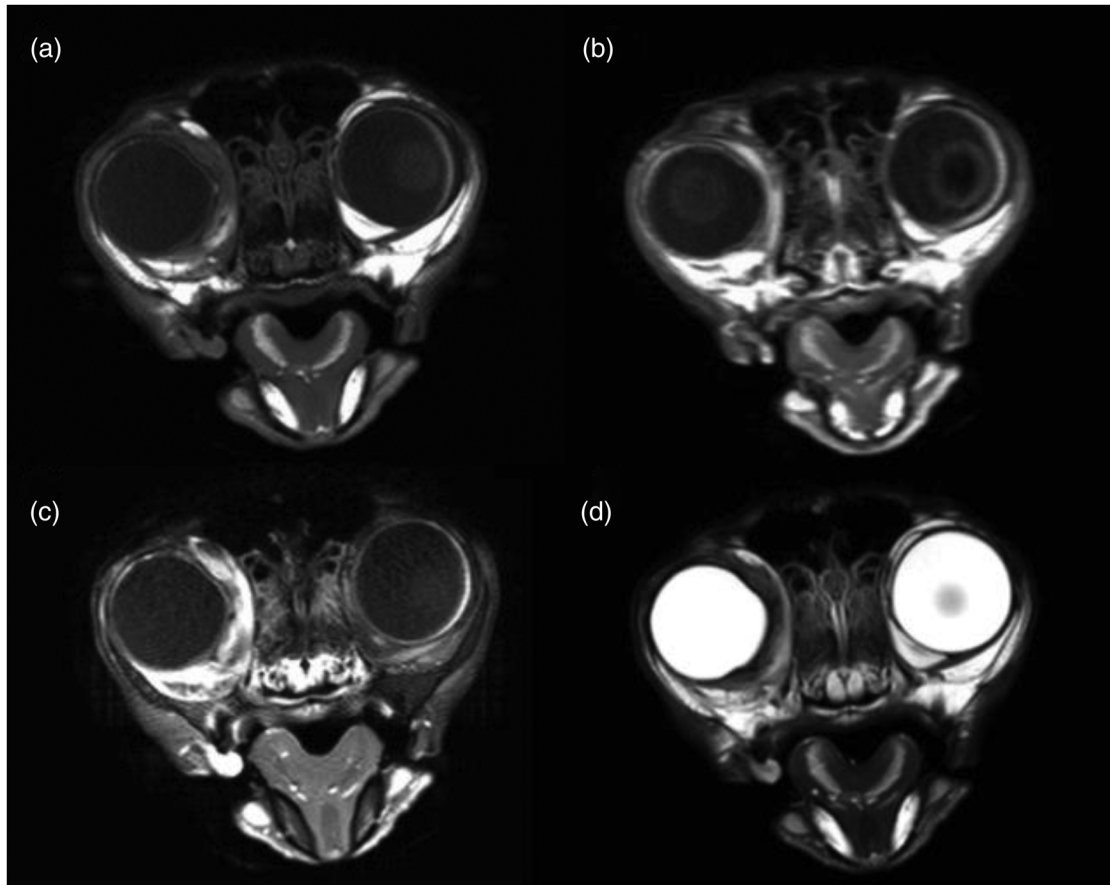


**FIGURE 3** The second magnetic resonance imaging (MRI) scan images, approximately 1 month after the first MRI scan. (a) T1-weighted sequence image. (b) T1-weighted contrast enhancement sequence image. (c) T1-weighted fat suppression sequence image. (d) T2-weighted sequence image. Compared with the first MRI images, the T2-weighted signal intensity and extent of contrast enhancement of the right periorbital tissue decrease. And the diameter of the extraocular muscle decreases as well

apparent. After 3 weeks of steroid therapy at the immunosuppressive dosage, the levels of serum alanine aminotransferase (2507.0 U/L) and aspartate aminotransferase (1230 U/L) were elevated, and poor spirit and appetite were noted. The decision of tapering the dosage of prednisolone gradually from 2 mg/kg/d to 1 mg/kg/d was made due to substantial adverse effects of high dosage of prednisolone. S-adenosyl-L-methionine at 33 mg/kg/day bid was then prescribed, and the dosage of prednisolone was further tapered from 1 mg/kg/day to 0.5 mg/kg/day in the following week.

The cat's spirit and appetite were improved after 1 week of supportive treatment and tapering the dosage of oral prednisolone. The retracted upper eyelid, keratitis and granulation of OD cornea progressed substantially (Figure 1c) during the period of tapering oral prednisolone. Because the long-term steroid therapy-related systemic complications were significant and no obvious clinical improvement was noted even under higher immunosuppressive dosage of steroid therapy, the decision of having the third MRI scan and right eye enucleation surgery was made 4 months after the first presentation.

The third MRI examination was performed approximately 2 months after the second MRI examination. No significant changes were found when compared with the second MRI examination except a periodon-

**TABLE 1** Comparison of the mean apparent diffusion coefficient (ADC) values of the three regions of interest (ROIs) between the abnormal right extraocular muscles (EOMs) and normal left EOMs in magnetic resonance imaging (MRI) scans

ADC value	Right EOMs	Left EOMs
First ROI	1.07	0.241
Second ROI	0.921	0.537
Third ROI	0.843	0.14

Note: Unit for ADC value is  $10^{-3}$  mm<sup>2</sup>/s.

tal mass was found in the right upper side of the oral cavity. Diffusion-weighted imaging (DWI) sequence and apparent diffusion coefficient (ADC) map were acquired for objective analysis of the EOMs. Three regions of interest (ROI) with the size of 2 mm<sup>2</sup> in bilateral EOMs in DWI images were outlined, and ADC measurements were calculated as shown in Table 1. The ADC values of the right EOMs were higher than the left ones. ADC values with the same size of two ROI in temporal muscles were 0.537 and 0.402  $10^{-3}$  mm<sup>2</sup>/s, both were lower than that of the right EOMs.



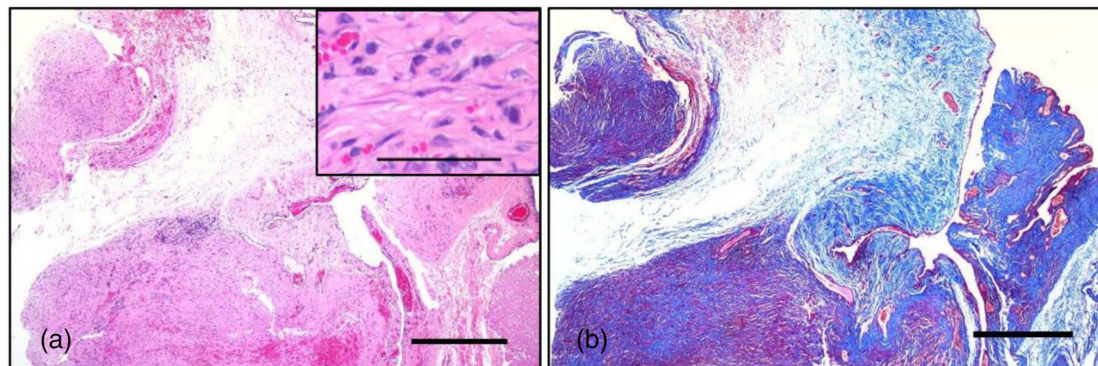


**FIGURE 4** Histopathological findings of the junction of periorbital tissue (P) and conjunctiva of upper eyelid (C) near the region of medial canthus of right eyeball. (a) Haematoxylin-eosin staining. Bar = 500  $\mu\text{m}$ . (b) Masson's trichrome staining. bar = 500  $\mu\text{m}$ . Within the dense collagenous fibrous stroma, there are loosely arranged scattered slender fibroblast-like cells along with congestion, haemorrhage, and minimal lymphocytic infiltration. Inset of (a): Showing scattered slender fibroblast-like cells embedded within the collagenous stroma. bar = 50  $\mu\text{m}$

Right eye enucleation surgery was performed by standard enucleation approach under general anaesthesia. Increased thickness and stiffness of both upper and lower eyelids were noted at surgery. The right globe, abnormal periorbital tissue, and OD upper and lower eyelids were taken for histopathological examination. The surgical wound healed well, and no abnormality was noted in the follow-up revisits. The oral mass was excised at the other veterinary clinic several months after the enucleation. The histopathological diagnosis of the gingival mass was odontogenic fibroma. Five months after the enucleation, the follow-up telephone communication with the owner confirmed that there was no sign of recurrence of the disease in the right eye, and no abnormal clinical sign was noted in the left eye.

## 2.2 | Histopathological findings

Histopathological examination of the right globe, periorbital tissue, and upper and lower eyelids revealed no evidence of neoplastic transformation or infection. Multifocal to coalescent marked collagenous fibrosis was found in the upper and lower eyelids, anterior sclera and episcleral soft tissue, and periorbital tissue (Figure 4a). The upper and lower eyelids were the only places where the fibrosis extended into the superficial region of the underlying muscularis. Although mild proliferation of loosely arranged slender fibroblast-like cells was also seen in the fibrotic regions, particularly in the region around medial canthus (Figure 4a), no evidence of infiltration of more dense neoplastic spindle cells was found. Within the fibrotic regions, highlighted by Masson's trichrome staining (Figure 4b), there was also sporadic mild to moderate lymphocytic infiltration. The cornea of the right eye had multifocal to coalescent severe ulceration with apparent hyperplasia and keratinization of the remaining epithelium, marked fibroplasia, angiogenesis, and fibrosis, and minimal pigmentation in the underlying upper stroma. Additionally, there were multifocal severe neutrophilic infiltration and mild to moderate haemorrhage with some hemosiderin deposition, which was highlighted by Perls Prussian blue staining. Occasion-

ally, sections of hair shaft were observed within the severely ulcerated surface of the cornea. Mild focal lymphocytic infiltration, mild fibrosis, and severe oedema were noted in one side of the ciliary body. Formation of iridociliary cysts lined by single-layered pigmented cells was seen in the iris and ciliary body.

Immunohistochemical (IHC) staining for smooth muscle actin (SMA), vimentin, S-100 protein, and glial fibrillary acidic protein (GFAP) was performed. The result showed scattered to occasionally coalescent weak to evident SMA-positive foci in some of those areas displaying marked collagenous fibrosis with slender fibroblast-like cells under HE and Masson's trichrome staining. The affected tissues included the periorbital tissue, conjunctiva of upper eyelid, junction of upper and lower eyelids, and third eyelid (Figure 5a–d), and the SMA-positive foci were merely distributed in the region near the medial canthus. In addition, an apparent SMA-positive zone was also seen in the granulation zone of the upper stroma of the ulcerated cornea (Figure 5e). No SMA-positive foci were found in the skin of upper eyelid, both of the skin and conjunctiva of lower eyelid, the periorbital tissue of lateral canthus, and the perisclera and episclera. The aforementioned SMA-positive regions displayed less apparent vimentin positivity, minimal or no S-100 positivity, and no GFAP positivity.

## 3 | DISCUSSION

The progressive sclerosing orbital disease in cats has recently been renamed as feline restrictive orbital myofibroblastic sarcoma (FROMS), based on the aggressive neoplastic process of the disease affecting the orbital tissue (Bell et al., 2011). An early and accurate diagnosis for FROMS is important due to its progressive nature and poor prognosis. The common clinical signs of FROMS include ulcerative keratitis, lagophthalmos, thickened eyelid, restrictive mobility of eyelid, and reduced retropulsion of the globe (Bell et al., 2011). Owing to the malignant nature of FROMS, bilateral orbital and other tissue involvement would greatly impact the quality of life of the

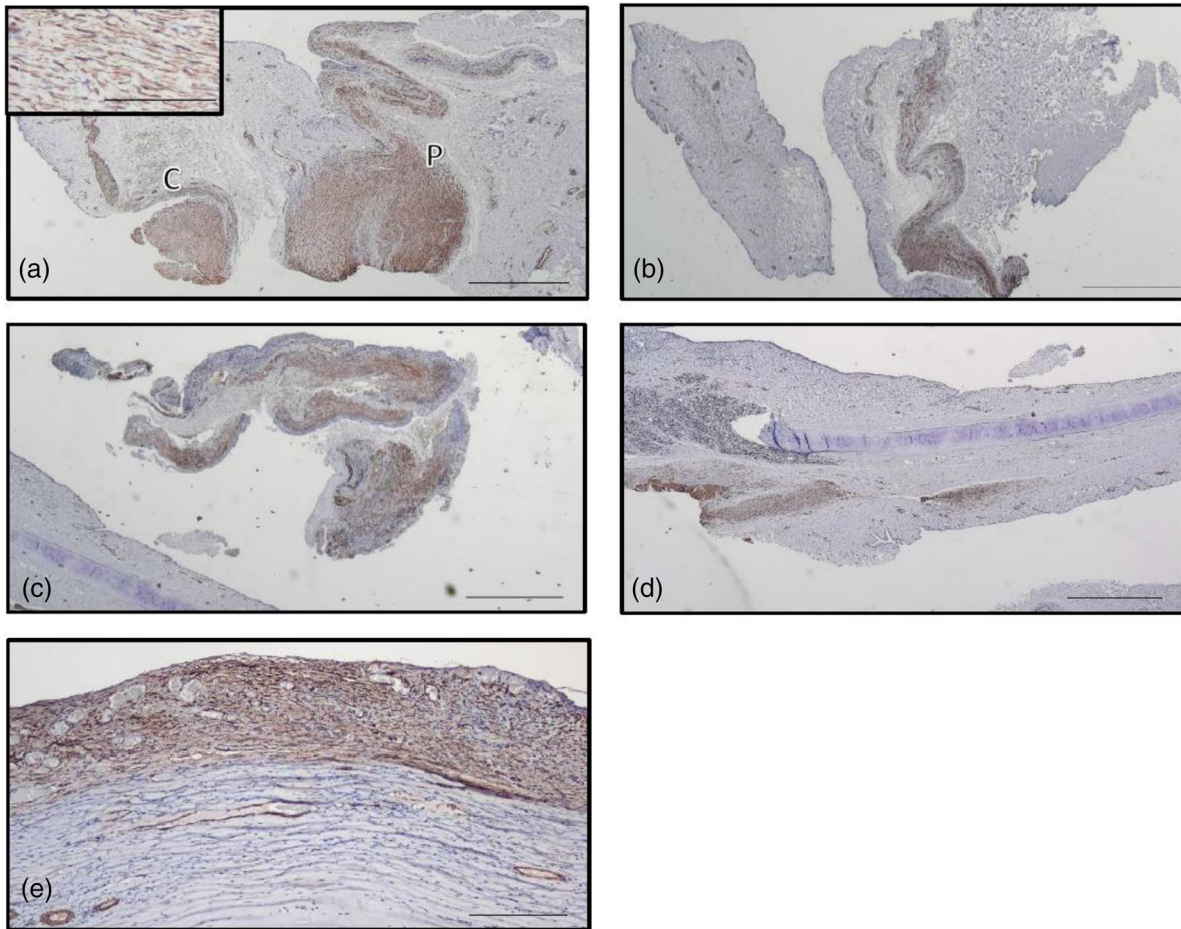


**FIGURE 5** Immunohistochemical staining results of smooth muscle actin (SMA). (a) Junction of periorbital tissue (P) and conjunctiva of upper eyelid (C) near the region of medial canthus of right eyeball. bar = 1000  $\mu\text{m}$ . (b) Soft tissue at the junction of upper and lower eyelids at the medial canthus aspect of right eyeball. bar = 1000  $\mu\text{m}$ . (c) Soft tissue of the base of third eyelid at the medial canthus aspect of right eyeball. bar = 1000  $\mu\text{m}$ . (d) Third eyelid of right eyeball. bar = 1000  $\mu\text{m}$ . (e) Cornea of right eyeball. bar = 200  $\mu\text{m}$ . Scattered to occasionally coalescent SMA-positive foci are randomly distributed in the regions near the medial canthus of the periorbital tissue, conjunctiva of upper eyelid, junction of upper and lower eyelids, and third eyelid. A liner SMA-positive zone is also seen in the granulation zone of the upper stroma of the ulcerated cornea. Inset of (a): Showing higher magnification of SMA-positive cells. Bar = 200  $\mu\text{m}$

affected cats, and euthanasia is often chosen in the later stage of the disease.

In the present case, the level of the right eyelid retraction and periorbital stiffness still progressed gradually even under the oral prednisolone management. No local invasion and/or infiltration to the surrounding tissue as that seen in neoplastic lesions was noted in the serial MRI scans. No left eye involvement was noted via clinical examination and MRI images. The gradually progressed corneal granulation and keratitis might be caused by the worsened lagophthalmos.

Although the clinical presentations with the retracted eyelid and reduced globe retropulsion were very similar to those of the previously reported FROMS cases, the course of the disease was not aggressive, and no bilateral involvement was seen in our case. We could not assure that the limited progress seen in our case was due to the steroid therapy or the nature course of the disease. However, there was obvious improvement in the periorbital swelling, globe retropulsion and previ-

ously persistent HIOP following oral prednisolone treatment, suggesting that there was possible involvement of inflammation in the disease.

The MRI findings of the FROMS-affected cat described by Thomasy et al. (2013) included mild thickening of the retrobulbar soft tissue lining and weakened signal of the retrobulbar fat; heterogenous hyperintensity of the left retrobulbar soft tissue was found in the short tau inversion recovery (STIR) image, and the thickened retrobulbar tissue showed no abnormal signal intensity in T1 and T2W images; the T1-weighted post-contrast images showed an increased signal intensity of the retrobulbar tissue.

In our case, the MRI showed markedly increased signal intensity of right EOMs, sclera, and cornea of right eye in T2W, FLAIR, and fat stat sequences accompanied with obvious contrast enhancement. It was found that the EOMs were enlarged, which may contribute to the diminished volume of retrobulbar adipose tissue. Considering the small size of the feline orbital structure, three-dimensional imaging

acquisition was chosen to provide better detail of the lesion. The slice thickness can be reduced significantly than that in conventional imaging, permitting high spatial resolution and lessening the likelihood of missing any insignificant lesions (Fleming et al., 2019). In the three scans, no mass was found in the retro- or peri-bulbar areas. And despite the enlargement, the alignment and contour of the extraocular muscle bundles were mostly unchanged, which were different from that found in the previous case report (Thomasy et al., 2013).

DWI and ADC maps were acquired, and increased ADC values of the right EOMs were measured. DWI is a technique that measures the random motion of water molecules in tissue and can be quantified by the ADC. DWI and ADC maps were used in human medicine helping distinguish orbital tumour and inflammation, or differentiate benign and malignant soft tissue tumours. Increased cell density and decreased extracellular space in malignant tumours will hinder the movement of water molecules and therefore have decreased ADC values (Wang et al., 2021). Also, the tumour stroma produced by activated fibroblasts was found to be inversely correlated to ADC value (Hauge et al., 2017). Inflammatory or benign lesions due to its higher free water content will have less diffusion restriction and therefore will show high ADC values (Ferreira et al., 2018) as seen in our case. The imaging findings also reflect that in histopathological examination those lesions mostly limited in superficial regions with some loosely arranged fibroblasts, and the underlying muscularis were only mildly affected, in contrary to the extensive fibrosis and deep stroma infiltration of densely packed cell neoplastic cells found in Thomasy's case (Thomasy et al., 2013).

In human medicine, orbital inflammation can have a wide range of underlying aetiologies. It can be idiopathic, thyroid-associated orbitopathy, sarcoidosis, granulomatous with polyangiitis, IgG4-related disease, or sclerosing orbital inflammation. Sarcoidosis, granulomatous with polyangiitis, and IgG4-related disease are systemic and multi-organs involvement usually presented. Apart from the ocular lesions, our case had normal physical condition. The elevated hepatic indexes were reversible after dose reduction of glucocorticoids and supportive therapy, they were thus believed to be drug related. Thyroid-associated orbitopathy is an autoimmune condition of the orbit. Though extraocular muscles are the most common orbital structure involved, they are mostly affected bilaterally and symmetrically, with a typical fusiform configuration. Idiopathic sclerosing orbital inflammation (ISOI), previously thought to be the end stage of idiopathic orbital inflammation (IOI, previously called pseudotumor), is now considered a distinct pathologic entity with marked fibrosis present early in the disease (Pemberton & Fay, 2012). Due to the extensive fibrosis, ISOI shows a slightly enhancing, ill-defined mass, which is hypointense on T2W images without DWI restriction. On the other hand, some similarities of the MRI and histopathologic characteristics are shared in our case and human IOI. IOI affects especially the medial rectus followed by the superior and lateral recti, involving both the belly and the tendon, giving the muscle a tubular appearance (Ferreira et al., 2018). In an acute process, increased signal intensity in T2W images can be appreciated and it will decrease when the lesion is more chronic (Harris, 2006). In IOI, diffusion is not restricted, and contrast enhancement is presented. Fibrosis is frequently present at

pathological examination accompanied with chronic inflammatory infiltrates (Ferreira et al., 2018).

In regard to the treatment, topical or systemic antibiotics, anti-inflammatory or immunosuppressive dose of glucocorticoids, and anti-viral therapy were used in cats with FROMS and idiopathic sclerosing orbital pseudotumor. Besides these, one cat received adiation therapy. But the responses of all cases were considered poor (Billson et al., 2006, Bell et al., 2011, Thomasy et al., 2013). In human IOI, though most patients showed initial response to systemic corticosteroids, recurrence was not uncommon, and the rate was 52% in one study (Mombaerts et al., 1996). Another report found that additional immunosuppressive agents were required in 20% of IOI cases (Yuen & Rubin, 2003). External beam radiotherapy, antimetabolites, T cell /calcineurin inhibitors, alkylating agents, lymphocyte inhibitors, and tumour necrosis factor-alpha inhibitors have been used in limited case reports against refractory IOI (Yeşiltaş & Gündüz, 2018). Our cat's clinical signs and MRI findings improved initially while receiving corticosteroids. It is unknown whether a multi-modal immunotherapy provides a better outcome. But it may be worth trying, especially in the early stage of the disease before fibrosis increases and inflammation subsides.

There were multifocal to coalescent severe collagenous fibrosis and areas of mild to moderate lymphocytic infiltration in the anterior portion of the sclera and the adjacent episcleral soft tissue of the right eye, periorbital soft tissue, and both upper and lower eyelids. Although a small to moderate number of loosely arranged thin fibroblast-like cells were scattered within the fibrotic regions, no evidence of infiltration of more densely packed streaming bundles of spindle-shaped neoplastic cells as those described in FROMS-affected cats (Bell et al., 2011; Thomasy et al., 2013) was identified. In addition, IHC staining for SMA demonstrated only some, instead of all, of the fibrotic regions detected under HE and Masson's trichrome staining exhibiting scattered to occasionally coalescent positive foci of myofibroblast proliferation in our case. These SMA-positive foci were distributed mainly in the region near medial canthus. Moreover, the granulation zone in the upper stroma of the ulcerated cornea also displayed an apparent SMA positivity, indicating that significant myofibroblast proliferation may appear in wound healing as well. The IHC result further supports that our case is not similar to those cases of classic FROMS (Bell et al., 2011; Thomasy et al., 2013).

Myofibroblasts and fibroblasts are key players in tissue repair. Under normal physiological condition of wound healing, myofibroblasts disappear via apoptosis, resulting in a much less cellular scar (Darby et al., 2014). However, myofibroblasts may fail to undergo cell death and persist under certain circumstances and lead to the development of hypertrophic scarring or even neoplasm such as inflammatory myofibroblastic tumours (IMTs) in the human, high-grade myofibroblastic sarcoma in the dog, and FROMS in the cat (Bell et al., 2011; Darby et al., 2014; Hojo et al., 2012; Thomasy et al., 2013). Human inflammatory myofibroblastic tumour (IMT), formerly termed inflammatory pseudotumor, is a rare neoplasm of the mesodermal myofibroblasts (Gomez-Roman et al., 2000). Inflammatory pseudotumour is a generic term used to be applied to various neoplastic and



non-neoplastic lesions that share a common microscopic appearance composed of spindle cells with the presence of varying leukocytes (Darby et al., 2014). In 2020, the World Health Organization (WHO) reclassified IMT as a specific tumour form of fibroblastic and myofibroblastic tumours (FMTs), which comprise neoplastic mesenchymal cells with morphology resembling fibroblasts and/or myofibroblasts (Sbaraglia et al., 2021). Based on the tumour aggressiveness, FMTs can be subdivided into four categories, including benign, intermediate (locally aggressive), intermediate (rarely metastasizing), and malignant; currently, IMT is classified as the intermediate (rarely metastasizing) FMTs (Sbaraglia et al., 2021). Whether, similar to humans, cats also have various subtypes of neoplastic and non-neoplastic fibroblastic/myofibroblastic proliferative disorders requires further study to clarify.

The histopathological findings of the FROMS reported previously included orbital infiltration and invasion of the spindle cells and collagenous matrix along fascial planes, moderate to severe keratitis, and lymphoplasmacytic inflammation of the affected tissues (Bell et al., 2011). Mild to moderate neoplastic transformation and invasion with no apparent anisocytosis and anisokaryosis were seen in those reported cases. In the present case, there was no neoplastic transformation and/or infiltration in the granulation tissue along the fascia, suggesting that chronic irritation of unknown origin might be the cause for the severe collagenous fibrosis and the lymphocytic inflammation.

#### 4 | CONCLUSION

The course of the disease, the advanced MRI image findings, and the histopathological changes of the present case are different from those of the previously reported FROMS cases (Billson et al., 2006; Bell et al., 2011; Thomasy et al., 2013). No neoplastic transformation or infection was found, and no other local or systemic causes could be identified. Hence, idiopathic sclerosing orbital pseudotumor, similar to human IOI, may be a more suitable diagnosis for the current case. The immunosuppressive dosage of steroid therapy could effectively improve the clinical signs and reduce the inflammation of the periorbital tissue but could not reverse the fibrotic changes in the affected areas as seen in the second and third MRI images. MRI scanning was helpful for evaluating the progression and possibly the malignancy of orbital lesions. The utility of DWI and ADC map at early stage may be helpful to guide the treatment strategy and introduce multi-modal immunosuppressive therapy early in refractory cases.

#### ACKNOWLEDGEMENTS

The authors would like to thank the assistance of supporting staff of the Ophthalmology and Imaging Departments of the National Taiwan University Veterinary Hospital, of the Graduate Institute of Molecular and Comparative Pathobiology, and the ophthalmologists of the Vision Eyecare Center for Animals (VECA), Taipei, Taiwan.

#### CONFLICT OF INTEREST

The authors declare no conflict of interest.

#### ETHICS STATEMENT

The authors confirm that the ethical policies of the journal, as noted on the journal's author guidelines page, have been adhered to. No ethical approval was required due to the nature of this case report.

#### AUTHOR CONTRIBUTIONS

*Data curation, formal analysis, and investigation:* Hao Lee, Chih-Ching Wu, and Pei-Wen Liao. *Writing—original draft:* Hao Lee and Chih-Ching Wu. *Writing—review and editing and validation:* Chih-Ching Wu, K. Michael Chang, Victor Fei Pang, and Chung-Tien Lin. *Conceptualization and visualization:* K. Michael Chang. *Validation, visualization, supervision, and project administration:* Victor Fei Pang, Chung-Tien Lin. *Methodology and visualization:* Li-Ning Wei, Yi-Ying Wu, Man-Ha Chan, and Yi-Shan Chiang.

#### FUNDING

This work was not supported by any funding source or institution.

#### DATA AVAILABILITY STATEMENT

The data that support the findings of this study are available from the corresponding author upon reasonable request.

#### PEER REVIEW

The peer review history for this article is available at <https://publons.com/publon/10.1002/vms3.822>.

#### ORCID

Chung-Tien Lin  <https://orcid.org/0000-0003-4115-4762>

#### REFERENCES

- Bell, C., Schwarz, T., & Dubielzig, R. (2011). Diagnostic features of feline restrictive orbital myofibroblastic sarcoma. *Veterinary Pathology*, 48(3), 742–750.
- Billson, F. M., Miller-Michau, T., Mould, J. R., & Davidson, M. G. (2006). Idiopathic sclerosing orbital pseudotumor in seven cats. *Veterinary Ophthalmology*, 9(1), 45–51.
- Darby, I. A., Laverdet, B., Bonté, F., & Desmoulière, A. (2014). Fibroblasts and myofibroblasts in wound healing. *Clinical, Cosmetic and Investigational Dermatology*, 7, 301.
- Ferreira, T. A., Saraiva, P., Genders, S., Buchem, M., Luyten, G., & Beenakker, J. (2018). CT and MR imaging of orbital inflammation. *Neuroradiology*, 60(12), 1253–1266.
- Fleming, K. L., Maddox, T. W., & Warren-Smith, C. M. (2019). Three-dimensional T1-weighted gradient echo is a suitable alternative to two-dimensional T1-weighted spin echo for imaging the canine brain. *Veterinary Radiology & Ultrasound*, 60(5), 543–551.
- Gomez-Roman, J. J., Ocejo-Vinyals, G., Sanchez-Velasco, P., Nieto, E. H., Leyva-Cobian, F., & Val-Bernal, J. F. (2000). Presence of human herpesvirus-8 DNA sequences and overexpression of human IL-6 and cyclin D1 in inflammatory myofibroblastic tumor (inflammatory pseudotumor). *Laboratory Investigation*, 80(7), 1121–1126.
- Harris, G. J. (2006). Idiopathic orbital inflammation: A pathogenetic construct and treatment strategy: The 2005 ASOPRS Foundation Lecture. *Ophthalmic Plastic & Reconstructive Surgery*, 22(2), 79–86.
- Hauge, A., Wegner, C. S., Gaustad, J. - V., Simonsen, T. G., Andersen, L. M. K., & Rofstad, E. K. (2017). Diffusion-weighted MRI-derived ADC values reflect collagen I content in PDX models of uterine cervical cancer. *Oncotarget*, 8(62), 105682.



- Hojo, Y., Tsuchiya, T., Shiraki, A., Suzuki, K., Shibutani, M., & Mitsumori, K. (2012). High-grade myofibroblastic sarcoma of inguinal region in a dog. *Journal of Veterinary Medical Science*, 74(5), 625–628.
- Mombaerts, I., Goldschmeding, R., Schlingemann, R. O., & Koornneef, L. (1996). What is orbital pseudotumor? *Survey of Ophthalmology*, 41(1), 66–78.
- Pemberton, J. D., & Fay, A. (2012). Idiopathic sclerosing orbital inflammation: A review of demographics, clinical presentation, imaging, pathology, treatment, and outcome. *Ophthalmic Plastic & Reconstructive Surgery*, 28(1), 79–83.
- Rootman, J., McCarthy, M., White, V., Harris, G., & Kennerdell, J. (1994). Idiopathic sclerosing inflammation of the orbit: A distinct clinicopathologic entity. *Ophthalmology*, 101(3), 570–584.
- Sbaraglia, M., Bellan, E., & Dei Tos, A. P. (2021). The 2020 WHO classification of soft tissue tumours: News and perspectives. *Pathologica*, 113(2), 70.
- Thomasy, S. M., Cissell, D. D., Arzi, B., Vilches-Moure, J. G., Lo, W. Y., Wisner, E. R., Dubielzig, R. R., & Maggs, D. J. (2013). Restrictive orbital myofibroblastic sarcoma in a cat—Cross-sectional imaging (MRI & CT) appearance, treatment, and outcome. *Veterinary Ophthalmology*, 16, 123–129.
- Wang, Q., Xiao, X., Liang, Y., Wen, H., Wen, X., Gu, M., Ren, C., Li, K., Yu, L., & Lu, L. (2021). Diagnostic performance of diffusion MRI for differentiating benign and malignant nonfatty musculoskeletal soft tissue tumors: A systematic review and meta-analysis. *Journal of Cancer*, 12(24), 7399.
- Yeşiltaş, Y. S., & Gündüz, A. K. (2018). Idiopathic orbital inflammation: Review of literature and new advances. *Middle East African Journal of Ophthalmology*, 25(2), 71.
- Yuen, S. J. A., & Rubin, P. A. (2003). Idiopathic orbital inflammation: Distribution, clinical features, and treatment outcome. *Archives of Ophthalmology*, 121(4), 491–499.

**How to cite this article:** Lee, H., Wu, C.-C., Liao, P.-W., Michael Chang, K., Wei, L.-N., Wu, Y.-Y., Chan, M.-H., Chiang, Y.-S., Pang, V. F., & Lin, C.-T. (2022). Features of ophthalmic, magnetic resonance imaging, and histopathology of a feline case of idiopathic sclerosing orbital pseudotumor. *Veterinary Medicine and Science*, 8, 1352–1360. <https://doi.org/10.1002/vms3.822>